LETTERS

TRIC channels are essential for Ca^{2+} handling in intracellular stores

Masayuki Yazawa[1,2], Christopher Ferrante[3], Jue Feng[2], Kazuhiro Mio[4], Toshihiko Ogura[4,5], Miao Zhang[1,2], Pei-Hui Lin[3], Zui Pan[3], Shinji Komazaki[6], Kazuhiro Kato[2], Miyuki Nishi[1,2], Xiaoli Zhao[3], Noah Weisleder[3], Chikara Sato[4], Jianjie Ma[3] & Hiroshi Takeshima[1,2]

Cell signalling requires efficient Ca^{2+} mobilization from intracellular stores through Ca^{2+} release channels, as well as predicted counter-movement of ions across the sarcoplasmic/endoplasmic reticulum membrane to balance the transient negative potential generated by Ca^{2+} release[1–7]. Ca^{2+} release channels were cloned more than 15 years ago[8,9], whereas the molecular identity of putative counter-ion channels remains unknown. Here we report two TRIC (trimeric intracellular cation) channel subtypes that are differentially expressed on intracellular stores in animal cell types. TRIC subtypes contain three proposed transmembrane segments, and form homo-trimers with a bullet-like structure. Electrophysiological measurements with purified TRIC preparations identify a monovalent cation-selective channel. In TRIC-knockout mice suffering embryonic cardiac failure, mutant cardiac myocytes show severe dysfunction in intracellular Ca^{2+} handling. The TRIC-deficient skeletal muscle sarcoplasmic reticulum shows reduced K^+ permeability, as well as altered Ca^{2+} 'spark' signalling and voltage-induced Ca^{2+} release. Therefore, TRIC channels are likely to act as counter-ion channels that function in synchronization with Ca^{2+} release from intracellular stores.

In the course of screening membrane proteins participating in cellular Ca^{2+} handling[10,11], we identified a protein with a calculated molecular mass of 33,300 from rabbit skeletal muscle, and named it TRIC type A (TRIC-A; also known as mitsugumin 33). Homology searches in databases revealed an additional structural homologue named TRIC-B. TRIC subtypes show fragmentary sequence identities, as determined by our complementary DNA and *in silico* cloning from various animal species (Supplementary Fig. 1). Northern blotting indicated that TRIC-A is preferentially expressed in excitable tissues, including striated muscle and brain, whereas TRIC-B is present in most mammalian tissues (Fig. 1a). Western blotting of fractionated muscle membranes suggested that TRIC-A is distributed throughout the sarcoplasmic reticulum (SR) but not in the cell-surface membranes (Fig. 1b). In further immunochemical studies, antibodies to TRIC-A decorated the SR and nuclear membranes in skeletal muscle, and TRIC-B behaved as an endoplasmic reticulum (ER)-resident protein in the brain tissues (Supplementary Fig. 1). Therefore, TRIC subtypes are localized to membrane systems associated with intracellular Ca^{2+} stores.

TRIC subtypes show conserved hydropathicity profiles that suggest multiple transmembrane segments (Fig. 1c). In limited proteolysis analysis using membrane vesicles (Supplementary Fig. 2), we found that the amino terminus of TRIC-A is located in the SR/ER lumen, whereas the carboxy terminus of TRIC-A is exposed to the cytoplasm. Further analysis of epitope-tagged recombinant proteins predicted three transmembrane segments in TRIC-A, and also detected the hydrophobic loop as a candidate for an ion-conducting pore between the first and second transmembrane segments. The proposed topology of TRIC subtypes (Fig. 1d) bears an overall resemblance to that of glutamate receptor channels[12].

Affinity chromatography using monoclonal antibodies allowed us to obtain pure TRIC-A protein (>95% purity) from muscle microsomal preparations solubilized with *n*-dodecyl β-D-maltoside (DDM) or digitonin (Supplementary Fig. 3). Treatment of TRIC-A with several chemical crosslinkers generated products with sizes corresponding to dimeric and trimeric assemblies (Fig. 1e and Supplementary Fig. 3). When purified TRIC-A was labelled with colloidal-gold-conjugated Fab fragments, electron microscopy frequently detected antigen–antibody complexes carrying three immunogold particles that protruded at near equal angular intervals (Fig. 1f). Combined computer algorithms, which collect, classify and average negatively stained electron-microscope images to reconstruct a three-dimensional volume[13–16], and the tilt series of the particle images, demonstrated that TRIC-A forms an elongated triangular pyramidal structure (Fig. 1g and Supplementary Figs 4 and 5). Thus, TRIC subtypes form a homo-trimeric structure, as in the cases of the P2X (ref. 17) and bacterial porin channels[18].

Using lipid bilayer reconstitution studies, we observed a functional cation-selective channel with TRIC-A purified from skeletal muscle (Fig. 2a, b). In a recording solution composed of 200 mM KCl (*cis*)/50 mM KCl (*trans*) (see Methods), a slope conductance of 110 ± 14 pS and a reversal potential of -20 ± 1.7 mV were observed, indicating the cation-selective nature of the TRIC-A channel (Fig. 2f). Although the single channel conductance properties of TRIC-A are similar to those of the SR K^+ channel reported previously[5,19], other characteristics suggest that the TRIC-A channel might represent a separate channel moiety. First, under bi-ionic conditions of 200 mM KCl (*cis*)/200 mM NaCl (*trans*), outward current was measured at a holding potential of 0 mV, which reverses at a potential of −10 mV (Fig. 2c). This negative reversal potential corresponds to moderate selectivity for K^+ over Na^+ (permeability ratio of $P_K/P_{Na} = 1.5$), which contrasts to the high K^+ selectivity of the SR K^+ channel[5,19]. Second, the SR K^+ channel is highly sensitive to inhibition by decamethonium[5], whereas the TRIC-A channel is insensitive to this drug at concentrations up to 100 μM (Fig. 2a). Furthermore, application of either $CaCl_2$ or $MgCl_2$ to the recording solutions did not significantly affect the reversal potential or open probability, indicating that the TRIC-A channel is impermeable and insensitive to divalent

[1]Department of Biological Chemistry, Graduate School of Pharmaceutical Sciences, Kyoto University, Kyoto 606-8501, Japan. [2]Department of Medical Chemistry, Graduate School of Medicine, Tohoku University, Miyagi 980-8575, Japan. [3]Department of Physiology and Biophysics, Robert Wood Johnson Medical School, New Jersey 08854, USA. [4]Neuroscience Research Institute, National Institute of Advanced Industrial Science and Technology (AIST), Ibaraki 305-8568, Japan. [5]PRESTO, Japan Science and Technology Agency, Saitama 332-0012, Japan. [6]Department of Anatomy, Saitama Medical University, Saitama 350-0495, Japan.

cations such as Ca^{2+} and Mg^{2+} (Supplementary Fig. 6). It is likely that TRIC channels either depend on putative interacting partners for certain characteristics, or represent an SR/ER channel that has not been previously reported.

As in the native specimens, the homo-trimeric assembly was also detected in epitope-tagged TRIC-A prepared from bacterial culture (Supplementary Fig. 3). This recombinant TRIC-A also formed a cation channel with kinetic properties indistinguishable from those of the native protein (Fig. 2d, f). Moreover, the application of monoclonal antibody against the C terminus of TRIC-A blocked the channel activity of both recombinant and native TRIC-A preparations (Fig. 2d, e), indicating that the observed channels are unlikely to result from minor impurities in our preparations.

To examine the physiological role of TRIC channels, we generated knockout mice (Supplementary Fig. 7). Mutant mice lacking *Tric-a* were viable and fertile, whereas mutant mice lacking *Tric-b* showed neonatal lethality. By crossing them, double-knockout mice lacking both subtypes (TRIC-DKO) and *Tric-a*$^{+/-}$*Tric-b*$^{+/-}$ (TRIC-DHE) mice were generated. TRIC-DKO mice exhibited a weak heartbeat at embryonic day (E) 9.5 and subsequent loss of cardiomyocyte viability (Supplementary Fig. 8), leading to terminal embryonic cardiac lethality beyond E10.5 (Fig. 3a). This aggravated lethality indicates that TRIC subtypes share complementary physiological functions. In the looped cardiac tubes from E8.5–9.5 TRIC-DKO embryos, irregular cytoplasmic vacuoles were formed, in particular within the ventricular myocytes (Fig. 3b). Electron microscopy revealed extensively swollen SR/ER structures in TRIC-DKO cardiomyocytes, resulting in the loss of normal rough and smooth ER structures (Fig. 3b and Supplementary Fig. 9). Using fixative solutions supplemented with oxalate to visualize high Ca^{2+} content in intracellular organelles[20], we frequently observed electron-dense Ca-oxalate deposits in the bloated SR/ER in TRIC-DKO myocytes, but not in TRIC-DHE myocytes (Fig. 3c).

Fluorometric Ca^{2+} imaging of TRIC-DKO cardiomyocytes revealed that the amplitudes of spontaneous Ca^{2+} oscillations were remarkably depressed at E8.5, illustrating compromised intracellular Ca^{2+} signalling associated with ablation of TRIC subtypes (Fig. 3d).

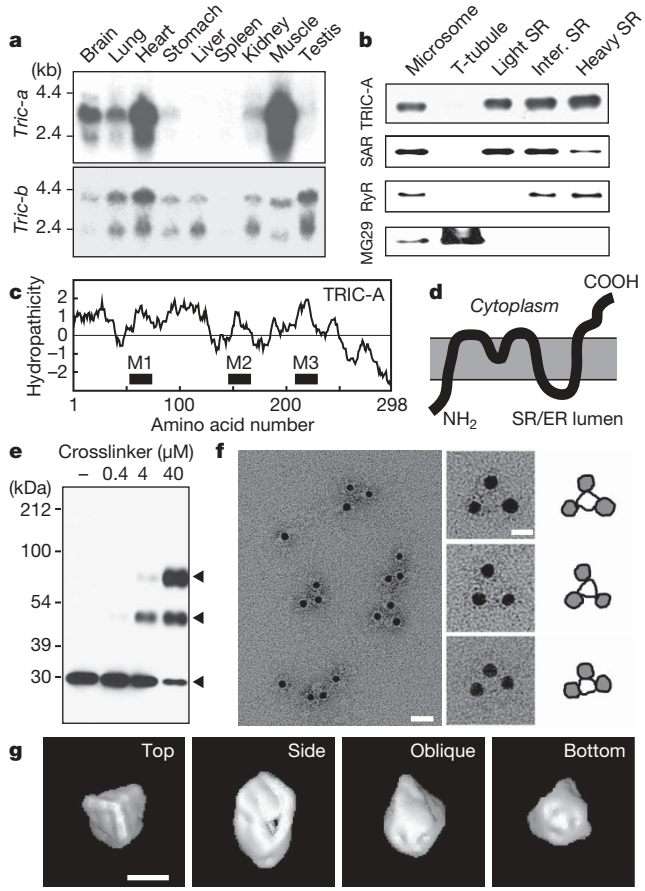

Figure 1 | Biochemical characterization of TRIC subtypes. **a**, Northern analysis of *Tric* subtypes in total RNA preparations (25 μg) from adult mice. **b**, Western analysis in rabbit skeletal muscle membrane preparations (total microsome, T-tubule, light SR, intermediate SR and heavy SR fractions; 2.5 μg) using antibodies to TRIC-A, sarcalumenin (SAR, longitudinal SR marker), ryanodine receptor (RyR, heavy SR marker) and mitsugumin 29 (MG29, T-tubular marker). **c**, Hydropathicity profile of TRIC-A in the Kyte–Doolittle algorithm (window size, 19 residues). M1–M3, putative transmembrane segments. **d**, Topology model of TRIC-A proposed in Supplementary Fig. 2. **e**, Chemical crosslinking of TRIC-A with 1,11-bis-maleimidotetraethyleneglycol. Arrowheads, monomeric, dimeric and trimeric forms. **f**, Electron microscopy images of native TRIC-A bound with gold-conjugated Fab fragment (left panel; scale bar, 200 Å). High-magnification images of the immuno-complexes and their contours are also shown (right panels; scale bar, 100 Å). **g**, Surface representations of three-dimensional reconstruction of native TRIC-A. Scale bar, 50 Å.

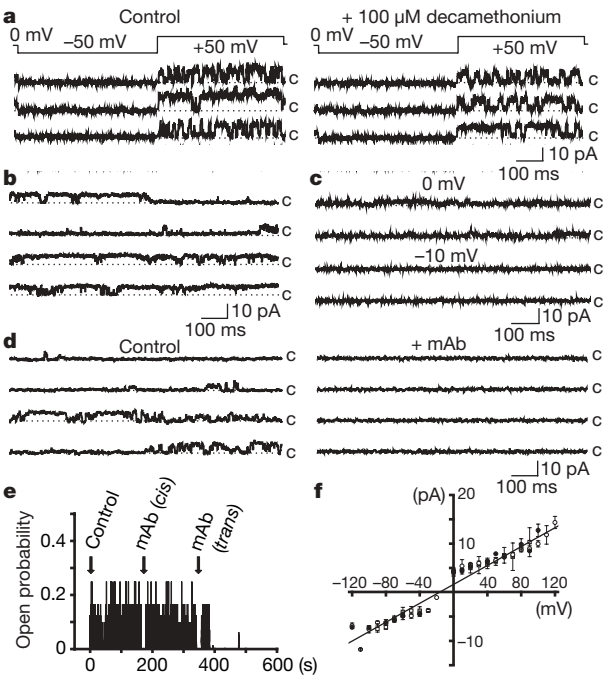

Figure 2 | Electrophysiological characterization of the TRIC-A channel. **a**, Single-channel recording of native TRIC-A purified using digitonin with 300:50 mM KCl (*cis*:*trans*) as the current carrier. Representative traces are shown from experiments in the absence (control, $n = 24$) or presence of 100 μM decamethonium ($n = 11$). The closed state (c) is marked with dashed lines. **b**, Current traces of native TRIC-A channel purified with DDM was recorded in a 200:50 mM KCl solution at a holding potential of 0 mV ($n = 12$). **c**, Under bi-ionic conditions of 200 mM KCl (*cis*)/200 mM NaCl (*trans*), TRIC-A current was measured at a holding potential of 0 mV, and became zero at −10 mV ($n = 5$). **d**, Channel activity from recombinant TRIC-A protein was recorded in a 200:50 mM KCl solution at a holding potential of 0 mV (control). In this recording, application of monoclonal antibody MY474 (20 μg ml^{-1}) to the *trans* solution led to complete closure of the channel (+mAb). **e**, Open probability diary plot illustrates that the recombinant TRIC-A channel was sensitive to blockade by MY474 from the *trans* side, as application to the *cis* side has no effect ($n = 3$). In other experiments, addition of the antibody to the *cis* solution could also block the TRIC-A channel ($n = 3$), owing to the reversal of channel orientation in the lipid bilayer. Similar effects of monoclonal antibody were observed in native TRIC-A channels (*cis* effect, $n = 3$, and *trans* effect, $n = 3$). **f**, Current–voltage relationships of native TRIC-A channels purified using digitonin (open circles) or DDM (open squares), and recombinant TRIC-A channels (filled circles) were obtained in a 200:50 mM KCl solution. Solid line represents a slope conductance of 110 ± 14 pS, with a reversal potential of −20.0 ± 1.7 mV (means ± s.e.m.).

Interestingly, TRIC-DKO myocytes displayed significantly larger caffeine-evoked Ca^{2+} transients than the TRIC-DHE myocytes (Fig. 3e). Because caffeine opens ryanodine receptor (RyR) channels and triggers Ca^{2+} release[21,22], the elevated caffeine-evoked Ca^{2+} transients suggest the SR/ER in TRIC-DKO cardiomyocytes is overloaded with Ca^{2+}, consistent with the Ca-oxalate deposits observed by electron microscopy. In Ca^{2+}-induced Ca^{2+} release (CICR) during cardiac excitation–contraction coupling, Ca^{2+} influx through dihydropyridine-sensitive channels (DHPR) activates the cardiac subtype of RyR (RyR2)[21–23]. In embryonic cardiomyocytes bearing immature intracellular stores, spontaneous Ca^{2+} oscillations are primarily produced by Ca^{2+} influx, with RyR2-mediated CICR acting to amplify Ca^{2+} signalling[20,24]. Both TRIC-DKO and RyR2-knockout mice display similar cardiac arrest phenotypes and share the swollen and overloaded SR/ER in embryonic cardiomyocytes[20]. These nearly identical pathologies, coupled with the observation that the E8.5 TRIC-DKO hearts retained normal expression of major Ca^{2+} store-related proteins, including RyR2, DHPR, SR/ER Ca^{2+}-ATPase (SERCA) and Na^+/Ca^{2+}-exchanger (Supplementary Fig. 8), suggest that depressed RyR2-mediated CICR weakens spontaneous oscillations and probably generates SR Ca^{2+} overloading in TRIC-DKO cardiomyocytes.

To examine the contribution of TRIC channels to Ca^{2+} signalling in skeletal muscle, we used osmotic stress to induce Ca^{2+} sparks, the elemental events of SR Ca^{2+} release, in isolated adult skeletal muscle fibres[25,26]. Line-scan imaging (Fig. 4a, b) detected a significant difference in Ca^{2+} spark amplitude between wild-type (WT) mice ($\Delta F/F_0 = 1.06 \pm 0.01$) and *Tric-a*$^{-/-}$-*Tric-b*$^{+/-}$ (mutant) mice (0.66 ± 0.01). In addition, the full duration at half maximum of Ca^{2+} sparks increased from 230 ± 17 ms in WT muscle to 301 ± 17 ms in mutant muscle ($P < 0.005$), probably reflecting a reduced Ca^{2+}-dependent inactivation mechanism of skeletal muscle RyR (RyR1)[3,21,22] associated with the impaired Ca^{2+} spark signalling. Using the silicone-grease embedding method to measure voltage-induced Ca^{2+} release (VICR) in muscle fibres[3,21,27], we examined the kinetic properties of SR Ca^{2+} release invoked by depolarization pulses to –20 mV from a holding potential of –80 mV. The kinetics of VICR was significantly slower in mutant muscle compared to WT muscle (Fig. 4c, d), indicating that TRIC deficiency leads to compromised SR Ca^{2+} release in skeletal muscle. We also found that the amplitudes of VICR were similar between WT ($\Delta F/F_0 = 2.48 \pm 0.08$) and mutant ($2.58 \pm 0.14$, $P = 0.52$) muscles, which would be expected because the amplitude of VICR at submaximal stimulation (−20 mV test pulse) is dependent on the recruitment of multiple RyRs to produce global Ca^{2+} release, whereas the effects of counter-current activity on Ca^{2+} release can be more effectively resolved at the level of individual Ca^{2+} sparks (Fig. 4a).

To test directly the contribution of TRIC channels to ionic permeability across the SR, we monitored the changes in membrane potential using a fluorescent voltage indicator, di-8-ANEPPQ. In SR vesicles prepared from hindlimb muscle and Ca^{2+}-loaded under ATP-containing conditions, the fluorescent dye detected a slightly negative potential of the luminal side, which was enhanced by thapsigargin-induced Ca^{2+} leak and counteracted by the K^+ ionophore, valinomycin (Fig. 4e, f). Membrane potential was significantly elevated under both resting/Ca^{2+}-loaded and thapsigargin-induced leak conditions in SR vesicles prepared from *Tric-a*$^{-/-}$ mice (Fig. 4f). This elevated potential was largely abrogated by valinomycin (Fig. 4g). Moreover, A23187, a Ca^{2+} ionophore, could return the elevated membrane potential in *Tric-a*$^{-/-}$ vesicles to similar levels observed in WT vesicles (data not shown). Taken together, TRIC-A deficiency seems to reduce K^+ permeability without affecting the basal Ca^{2+} permeability across the SR membrane, consistent with the monovalent-cation-selective nature of the TRIC-A channel (Fig. 2).

TRIC channels seem to predominantly be permeated by K^+ under intracellular conditions. Results from our mutant mice indicate that TRIC channels support RyR2-mediated CICR in cardiomyocytes and RyR1-mediated VICR in skeletal muscle, by providing certain aspects of the physiological mechanism for counter-ion movement during rapid SR/ER Ca^{2+} release (Fig. 4h). In addition to TRIC channels, other molecular components may also contribute to this mechanism, as caffeine-evoked Ca^{2+} release remains active in TRIC-DKO cardiomyocytes and VICR is only partially compromised in TRIC-deficient skeletal muscle. For example, as a cation-selective channel

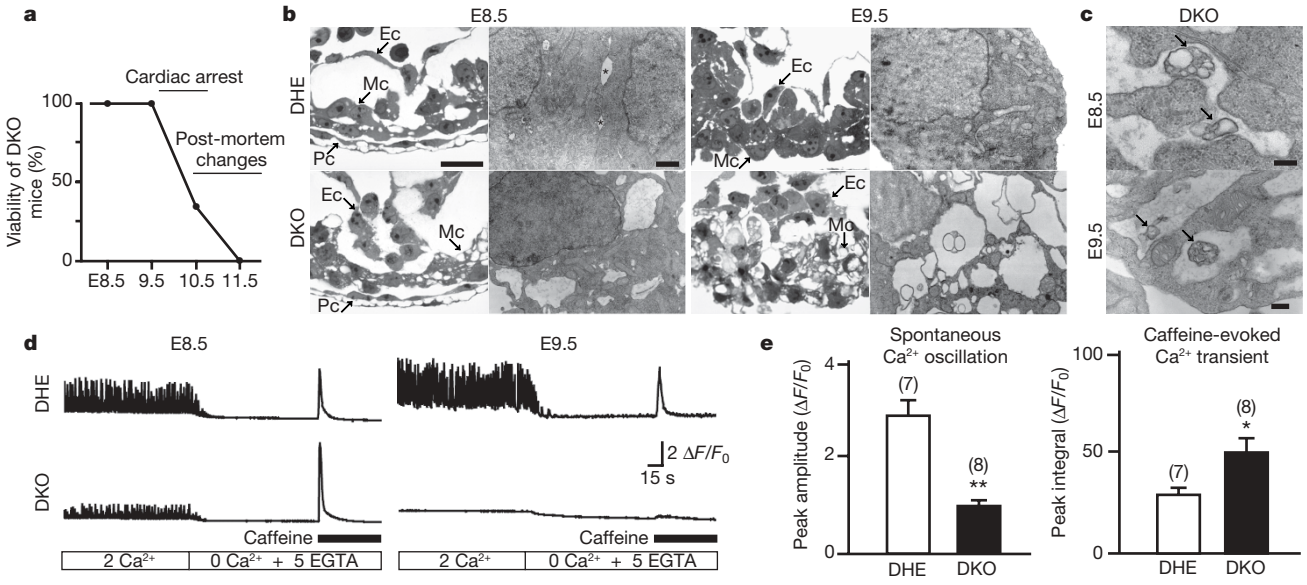

Figure 3 | Physiological abnormalities in TRIC-knockout hearts. a, TRIC-DKO embryos exhibited weak heartbeats at E9.5, stopped beating at ~E10.5, and post-mortem autolysis at ~E11.5. **b**, Histological and ultrastructural abnormalities in TRIC-DKO embryonic hearts. Pc, pericardium; Mc, myocardium; Ec, endocardium; asterisks, intercellular space. Representative data from at least three embryos are shown. Scale bars, 20 μm (left panels) and 1 μm (right panels). **c**, Formation of Ca-oxalate deposits (arrows) in the swollen SR/ER of TRIC-DKO cardiomyocytes. No such precipitates were observed in control embryos. Scale bar, 0.2 μm. **d**, Fluo-4 Ca^{2+} imaging of TRIC-DKO cardiomyocytes in bathing solutions containing 2 mM $CaCl_2$, 5 mM EGTA or 20 mM caffeine. Representative data from at least seven embryos are shown. **e**, Weak spontaneous Ca^{2+} oscillations and enhanced caffeine-evoked Ca^{2+} transients in E8.5 TRIC-DKO cardiomyocytes. Data represent the mean ± s.e.m., and *n* values are shown in parentheses. $^*P < 0.05$ and $^{**}P < 0.01$ in *t*-test.

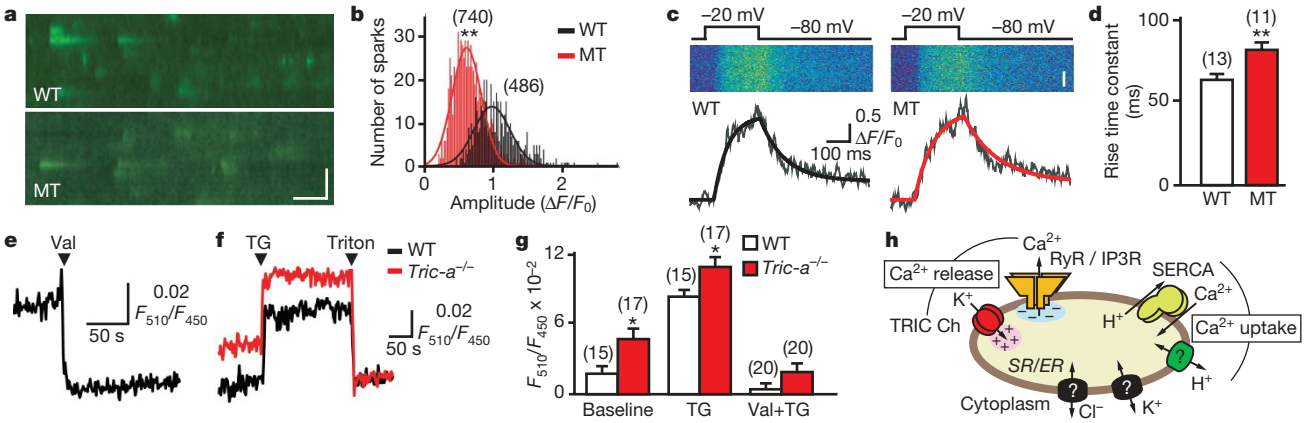

Figure 4 | Compromised Ca^{2+} release and altered membrane potential in TRIC-deficient skeletal muscle SR. **a**, Ca^{2+} spark images from wild type (WT) and *Tric-a*$^{-/-}$*Tric-b*$^{+/-}$ mutant (MT) skeletal muscle fibres. Scale bars, 10 μm and 2 s. **b**, Amplitude histogram of Ca^{2+} sparks were fitted with a gaussian distribution function. **c**, Measurement of VICR in WT and MT fibres under voltage-clamp conditions. Scale bar, 3 μm. Fluorescence traces were fitted by two exponential functions (black and red lines) with rise time constants of 55.3 ms for WT and 76.8 ms for MT. **d**, The rise time constant for VICR in MT fibres (81.9 ± 4.5 ms) was significantly elevated above WT controls (63.9 ± 3.0 ms). **e**, Fluorometric measurements of SR membrane potential using di-8-ANEPPQ. Decrease in the fluorescence ratio following addition of valinomycin (Val, 1 μM) reflects K^+ influx into WT SR vesicles. **f**, Inhibition of SERCA activity by thapsigargin (TG, 2 μM) induced Ca^{2+} leakage and enhanced negative potential across SR vesicles. Data were normalized to levels after the addition of Triton X-100 (0.2%). **g**, Summary data for di-8-ANEPPQ fluorescence at initial levels under Ca^{2+}-loaded conditions (Baseline) and following TG application and Val+TG application. The data in **b**, **d** and **g** are presented as mean ± s.e.m. and *n* values are shown in parentheses. $^*P < 0.05$ and $^{**}P < 0.01$ in *t*-test or ANOVA. **h**, Proposed role of TRIC channels in Ca^{2+} handling of intracellular stores. Physiological Ca^{2+} release mediated by RyR and IP3-receptor (IP3R) channels probably requires counter-ion movement to neutralize the accumulation of transient negative potential across the SR/ER. Compromised Ca^{2+} spark signalling and VICR in TRIC-deficient muscle indicate that permeation of K^+ or Na^+ through TRIC channels probably contributes to this mechanism. Several H^+, K^+ or Cl^--selective channels were proposed on the ER/SR from electrophysiological and biochemical data, but their molecular identities and biological functions remain to be elucidated.

conducting both Ca^{2+} and monovalent cations[3,22], RyR channels may contribute to both Ca^{2+} release and counter-ion permeation while locked in an open state. SERCA is responsible for Ca^{2+} uptake and catalyses Ca^{2+} and H^+ counter-transport[28], which is probably supported by the high H^+ permeability across the SR/ER membrane[29]. In addition, several K^+ and Cl^--selective channels on the SR/ER that were previously identified by other investigators[5,30] could also participate in neutralizing the transient negative membrane potential generated by Ca^{2+} release. Ubiquitously expressed TRIC channels seem essential for physiological Ca^{2+} release that regulates important cellular functions, and therefore could be unique targets in pharmaceutical or agrichemical applications.

METHODS SUMMARY

TRIC channel purification. Microsomal vesicles from rabbit skeletal muscle were solubilized with digitonin or DDM, and native TRIC-A protein was purified using an affinity column conjugated with monoclonal antibody MY474. Recombinant TRIC-A carrying both 6× histidine and haemagglutinin (HA) tags at the C terminus was purified from *Escherichia coli* through a combination of Ni^{2+}- and anti-HA affinity columns.

Electron microscopy analysis. Purified TRIC-A was decorated with immunogold labelled Fab fragments derived from antibody MY474 and analysed using electron microscopy. The three-dimensional image reconstruction of TRIC-A from negatively stained electron microscopy particle images was conducted by our established SPINNS method[13–15].

Lipid bilayer reconstitution. Electrophysiological characterization of TRIC-A preparations was conducted using conventional methods for lipid bilayer recordings[5,19]. Purified TRIC-A protein was added to the *cis* side of a lipid bilayer membrane formed with 50% phosphatidylserine and 50% phosphatidylethanolamine.

Knockout mouse production. TRIC-A and TRIC-B knockout mice were generated by our standard methods. TRIC-DKO embryos generated were subjected to anatomical, biochemical and Ca^{2+} imaging analyses[11,20].

Muscle Ca^{2+} measurements. Flexor digitorum brevis (FDB) fibres were isolated from adult mice, and Ca^{2+} sparks and VICR were monitored[25–27]. Muscle fibres were loaded with Fluo-4 AM, and Ca^{2+} signalling evoked by osmotic shock or depolarization was captured by line-scan imaging with a confocal microscope.

SR membrane potential measurements. SR vesicles prepared from mouse hindlimb muscle were resuspended in a Cl^--free solution supplemented with 0.5 μM di-8-ANEPPQ (Invitrogen). Potential-dependent fluorescence changes in response to valinomycin, thapsigargin, A23187 or TritonX-100 were monitored at an emission wavelength of 570 nm with dual excitation wavelengths of 450 and 510 nm. Quantitative changes in membrane potential were assayed by changes in the ratio of fluorescence intensity (F_{510}/F_{450}).

Full Methods and any associated references are available in the online version of the paper at www.nature.com/nature.

Received 27 November 2006; accepted 14 May 2007.

1. Ebashi, S. Excitation-contraction coupling. *Annu. Rev. Physiol.* **38**, 293–313 (1976).
2. Berridge, M. J. The endoplasmic reticulum: a multifunctional signaling organelle. *Cell Calcium* **32**, 235–249 (2002).
3. Fill, M. & Copello, J. A. Ryanodine receptor calcium release channels. *Physiol. Rev.* **82**, 893–922 (2002).
4. Somlyo, A. V., Shuman, H. & Somlyo, A. P. Composition of sarcoplasmic reticulum *in situ* by electron probe X-ray microanalysis. *Nature* **268**, 556–558 (1977).
5. Coronado, R. & Miller, C. Decamethonium and hexamethonium block K^+ channels of sarcoplasmic reticulum. *Nature* **288**, 495–497 (1980).
6. Fink, R. H. & Veigel, C. Calcium uptake and release modulated by counter-ion conductances in the sarcoplasmic reticulum of skeletal muscle. *Acta Physiol. Scand.* **156**, 387–396 (1996).
7. Meissner, G. Monovalent ion and calcium ion fluxes in sarcoplasmic reticulum. *Mol. Cell. Biochem.* **55**, 65–82 (1983).
8. Takeshima, H. *et al.* Primary structure and expression from complementary DNA of skeletal muscle ryanodine receptor. *Nature* **339**, 439–445 (1989).
9. Furuichi, T. *et al.* Primary structure and functional expression of the inositol 1,4,5-trisphosphate-binding protein P400. *Nature* **342**, 32–38 (1989).
10. Takeshima, H. *et al.* Mitsugumin29, a novel synaptophysin family member from the triad junction in skeletal muscle. *Biochem. J.* **331**, 317–322 (1998).
11. Takeshima, H. *et al.* Junctophilins: a novel family of junctional membrane complex proteins. *Mol. Cell* **6**, 11–22 (2000).
12. Dani, J. A. & Mayer, M. L. Structure and function of glutamate and nicotinic acetylcholine receptors. *Curr. Opin. Neurobiol.* **5**, 310–317 (1995).
13. Ogura, T. & Sato, C. Auto-accumulation method using simulated annealing enables fully automatic particle pickup completely free from a matching template or learning data. *J. Struct. Biol.* **146**, 344–358 (2004).
14. Ogura, T. & Sato, C. Automatic particle pickup method using a neural network has high accuracy by applying an initial weight derived from eigenimages: a new reference free method for single-particle analysis. *J. Struct. Biol.* **145**, 63–75 (2004).

15. Ogura, T., Iwasaki, K. & Sato, C. Topology representing network enables highly accurate classification of protein images taken by cryo electron-microscope without masking. *J. Struct. Biol.* **143,** 185–200 (2003).
16. van Heel, M. *et al.* Single-particle electron cryo-microscopy: towards atomic resolution. *Q. Rev. Biophys.* **33,** 307–369 (2000).
17. Mio, K. *et al.* Visualization of the trimeric $P2X_2$ receptor with a crown-capped extracellular domain. *Biochem. Biophys. Res. Commun.* **337,** 998–1005 (2005).
18. Cowan, S. W. *et al.* Crystal structures explain functional properties of two *E. coli* porins. *Nature* **358,** 727–733 (1992).
19. Liu, Q.-Y. *et al.* Reconstitution of the solubilized cardiac sarcoplasmic reticulum potassium channel identification of a putative M_r ~80 kDa polypeptide constituent. *FEBS Lett.* **291,** 13–16 (1991).
20. Takeshima, H. *et al.* Embryonic lethality and abnormal cardiac myocytes in mice lacking ryanodine receptor type 2. *EMBO J.* **17,** 3309–3316 (1998).
21. Endo, M. Calcium release from the sarcoplasmic reticulum. *Physiol. Rev.* **57,** 71–108 (1977).
22. Meissner, G. Ryanodine receptor/Ca^{2+} release channels and their regulation by endogenous effectors. *Annu. Rev. Physiol.* **56,** 485–508 (1994).
23. Fabiato, A. Calcium-induced release of calcium from the cardiac sarcoplasmic reticulum. *Am. J. Physiol.* **245,** C1–C14 (1983).
24. Antoon, F. M. *et al.* Presence of functional sarcoplasmic reticulum in the developing heart and its confinement to chamber myocardium. *Dev. Biol.* **223,** 279–290 (2000).
25. Wang, X. *et al.* Uncontrolled calcium sparks act as a dystrophic signal for mammalian skeletal muscle. *Nature Cell Biol.* **7,** 525–530 (2005).
26. Weisleder, N. *et al.* Muscle aging is associated with compromised Ca^{2+} spark signaling and segregated intracellular Ca^{2+} release. *J. Cell Biol.* **174,** 639–645 (2006).
27. Collet, C. *et al.* Intracellular calcium signals measured with indo-1 in isolated skeletal muscle fibers from control and *mdx* mice. *J. Physiol. (Lond.)* **520,** 417–429 (1999).
28. Toyoshima, C. & Inesi, G. Structural basis of ion pumping by Ca^{2+}-ATPase of the sarcoplasmic reticulum. *Annu. Rev. Biochem.* **73,** 269–292 (2004).
29. Meissner, G. & Young, R. C. Proton permeability of sarcoplasmic reticulum vesicles. *J. Biol. Chem.* **255,** 6814–6819 (1980).
30. Kourie, J. I. *et al.* Characteristics of two types of chloride channel in sarcoplasmic reticulum vesicles from rabbit skeletal muscle. *Biophys. J.* **70,** 202–221 (1996).

Supplementary Information is linked to the online version of the paper at www.nature.com/nature.

Acknowledgements We thank M. Kameyama for technical assistance, M. Fill and G. Meissner for suggestions, K. Hirose for close cooperation in electron microscopy studies, H. Masumiya for help with the lipid bilayer measurements, and T. Iwamoto for providing anti-NCX1 antibody. This work was supported in part by the Ministry of Education, Culture, Sports, Science and Technology of Japan, the Japan Science and Technology Agency, the Ministry of Health and Welfare of Japan, the Japan New Energy and Industrial Technology Development Organization, the Naito Foundation, the Sumitomo Foundation, the Uehara Memorial Foundation, the Takeda Science Foundation, and the National Institutes of Health.

Author Contributions M.Y., J.F. and M.Z. conducted biochemical experiments and characterized TRIC-DKO mice. K.M., T.O. and C.S. reconstructed the three-dimensional structure. M.Y., Z.P. and J.M. conducted bilayer measurements. C.F., P-H.L., N.W., X.Z. and J.M. characterized TRIC-deficient skeletal muscle. S.K. was responsible for histology. K.K., M.N. and H.T. identified TRIC subtypes and produced knockout mice. H.T. oversaw the project.

Author Information Reprints and permissions information is available at www.nature.com/reprints. Sequence data for rabbit and mouse TRIC channel cDNAs have been deposited in the DDBJ/NCBI/EMBL nucleotide databases under accession numbers of AB261158–AB261160.The authors declare no competing financial interests. Correspondence and requests for materials should be addressed to H.T. (takeshim@pharm.kyoto-u.ac.jp).

METHODS

TRIC channel purification. For purification of native TRIC-A, total microsomes were prepared from rabbit skeletal muscle[31] and solubilized in a buffer containing 1% DDM, 0.25 M sucrose, 2 mM 2-mercaptoethanol (2ME), 50 mM Tris-HCl (pH 7.4) and protease inhibitors. After the addition of NaCl (0.15 M in final concentration), insoluble materials were removed by ultracentrifugation and solubilized proteins were applied to Protein G Sepharose (Amersham Biosciences) crosslinking with monoclonal antibody MY474. After washing the resin with a buffer containing 0.1% DDM, 0.25 M sucrose, 2 mM 2ME, 0.3 M NaCl, 50 mM Tris-HCl (pH 7.4) and protease inhibitors, TRIC-A was eluted with the synthetic peptide (100 μM), which is composed of the rabbit TRIC-A C-terminal 19 residues carrying the antigenic epitope of antibody MY474. The peptide was removed by gel filtration (Superdex 200, Amersham Biosciences) with a running buffer containing 0.05% DDM, 0.25 M sucrose, 0.15 M NaCl, 20 mM NaPi (pH 7.0) and protease inhibitors. By using similar protocols, native TRIC-A was also prepared with digitonin as a detergent in place of DDM. These preparations were used in crosslinking experiments, lipid bilayer measurements and electron microscopy (EM) imaging analysis.

For production of recombinant protein, the cDNA fragment encoding rabbit TRIC-A carrying the C-terminal haemagglutinin (HA)-tag was subcloned into the pQE60 vector (Qiagen) for histidine-tagged protein expression. Cultured bacteria were treated with lysozyme and sonicated, and recombinant TRIC-A was then solubilized with 1% digitonin. After the removal of cellular debris, the lysate was applied to Ni-Sepharose (Amersham Biosciences), and recombinant protein was eluted with a buffer containing 0.1% digitonin, 20 mM NaP_i (pH 7.4), 0.5 M NaCl, 500 mM imidazole, 1 mM EDTA, 2 mM 2ME and proteinase inhibitors. The eluted solution was diluted to reduce the salt concentration and applied to anti-HA agarose (Sigma). After washing the resin, recombinant TRIC-A was recovered using a buffer containing 0.1% digitonin, 20 mM NaP_i (pH 7.4), 0.5 M NaCl, 0.1 mM EDTA, 0.1 mg ml^{-1} HA peptide (Sigma) and proteinase inhibitors. The peptide was removed by the Ni-Sepharose affinity chromatography and dialysis, and purified preparations were subjected to crosslinking and lipid bilayer experiments.

Membrane topology assay. Membrane vesicles were prepared from mouse skeletal muscle[32] and HEK293 cells[33] under isotonic conditions, and the transmembrane topology of the TRIC-A channel was examined as essentially described previously[34]. Membrane vesicles were suspended in the buffer containing 10 mM Hepes-KOH (pH 7.4), 100 mM NaCl, 10 mM KCl, 1.5 mM $MgCl_2$, 5 mM sodium EDTA, 5 mM sodium EGTA and 250 mM sucrose, and treated with varying concentrations of proteinase K in the absence or presence of 1% Triton X-100. The reactions were stopped by adding phenylmethylsulphonyl fluoride and the degradability of TRIC-A proteins was analysed by immunoblotting.

EM image analysis. Fab fragment was prepared from antibody MY474 using a commercially available kit (Immunopure Fab preparation kit, Pierce Biotechnology), reacted with colloidal gold particles (British BioCell International) and purified by gel filtration[35]. For the immuno-decoration, purified TRIC-A with DDM was reacted with the Fab fragment at a molecular ratio of 1:5. TRIC-A preparations with or without the immuno-decoration were then applied to thin carbon films, negatively stained with 2% uranyl acetate solution and analysed using an electron microscope (JEM-100CX, JEOL) at 55,100× magnification with a 100-kV acceleration voltage. Images were recorded on SO-163 films (Eastman Kodak) and digitized with a Scitex Leafscan 45 scanner (Leaf systems) at a pixel size of 1.82 Å at the specimen level.

Three-dimensional-structure reconstruction. We developed a single particle image analysis method using neural networks[14,15] and simulated annealing[13], namely SPINNS. For 3D reconstruction of the TRIC-A channel, image analysis was performed using combined SPINNS and IMAGIC V algorithms[16]. The TRIC-A projections were primarily selected in 100 × 100 pixel subframes using the auto-accumulation method with simulated annealing[13]. Selected 330 particles were rotated at 10° increments to generate 330 × 36 images, and they were used to train the three-layer pyramidal-type neural network[14]. The trained neural network further selected 10,998 particles and the obtained images were aligned rotationally and translationally[16,36] using the reference free method[14]. Because of the limited resolution, the contrast transfer function (CTF) correction was not performed in this analysis. The images were circularly masked with a diameter of 80 pixels to exclude the perimeter and sorted into 250 classes by the modified growing neural gas network method, which enables accurate and robust classification against noise because of its flexible neural network structure[15]. The resulting averages were used as new references and the cycle from alignment to classification was repeated 14 times. Next, the orientational Euler angles of the class averages were determined from the sinograms using cross-correlation functions[16] assuming a three-fold symmetry. They were used to calculate an initial 3D structure by the SIRT method[36]. The 3D map was further refined by the projection matching method for 10 cycles[36]. The FSC was used to assess the resolution of the final 3D map[37] at the threshold of 0.5.

Lipid bilayer measurements. Channel measurements were conducted as described previously[38]. Purified TRIC-A preparations (~0.2 μg) were added to the *cis* side of a lipid bilayer membrane formed across a 200-μm-diameter aperture. The lipid bilayer-forming solution contained 50% phosphatidylserine and 50% phosphatidylethanolamine (Avanti Polar Lipids) at a concentration of 40 mg ml^{-1} in *n*-decane (Sigma). Recording solutions were buffered at pH 7.4 with 10 mM HEPES-Tris. Channel recordings were made with Axopatch 200A patch-clamp unit (Axon Instruments), and the data were digitized at 1 kHz and filtered at 1 kHz (low-pass) using a 16 bit A/D-D/A converter and analysed with pClamp software (Axon Instruments).

Knockout mouse production. Knockout mice were generated using our standard methods[39] using J1 embryonic stem cells[40]. TRIC-DKO embryos generated were subjected to anatomical, biochemical and Ca^{2+} imaging analyses[11,20]. PCR primers used for mouse genotyping (Supplementary Fig. 7) were A-1 (TCAGTGGCGAGGGAGCATTCGTCG), A-2 (GTCCTCCTAACCGTAAACAAGAGC), B-1 (GTCATGGAGTACCCGTGGGATGATC) and B-2 (CCCTCTCCTGGTTCAACACGCTAGC).

Muscle Ca^{2+} measurements. Flexor digitorum brevis (FDB) fibres were isolated from adult mice, and Ca^{2+} sparks and VICR were monitored[25–27]. Muscle fibres were loaded with Fluo-4 AM, and Ca^{2+} signalling evoked by osmotic shock or depolarization was captured by line-scan imaging with a confocal microscope. For voltage clamp, major portions of both ends of the fibre were coated with silicone grease, and Ca^{2+} transients were elicited by repeated 200-ms test pulses to –20 mV from a holding potential of –80 mV.

SR membrane potential measurements. SR vesicles were prepared from 3–6-month-old hindlimb muscle from either wild-type ($n = 20$) or *Tric-a*$^{-/-}$ ($n = 13$) mice as described previously[31]. SR vesicles (60 μg protein) were resuspended in 2 ml Cl^--free SR-loading buffer (in mM: K glutamate 107.8, EGTA-KOH 2, $MgSO_4$ 6.6, ATP 5.4, creatine phosphate 15, Ca gluconate 0.98, BES-KOH 20, pH 7.2, free Ca^{2+} level of pCa = 6.6), supplemented with 0.5 μM di-8-ANEPPQ (Invitrogen) for 6 min at room temperature with constant stirring. Potential-dependent fluorescence changes in response to 1 μM valinomycin, 2 μM thapsigargin, 40 μM A23187 or 0.2% TritonX-100 were monitored in a DeltaRAM fluorometer (Photon Technology International) with an emission wavelength of 570 nm and a ratio of the excitation intensity of F_{510}/F_{450}.

31. Saito, A. *et al.* Preparation and morphology of sarcoplasmic reticulum terminal cisternae from rabbit skeletal muscle. *J. Cell Biol.* **99,** 875–885 (1984).
32. Fernandez, J. L., Rosemblatt, M. & Hidalgo, C. Highly purified sarcoplasmic reticulum vesicles are devoid of Ca^{2+}-independent ('basal') ATPase activity. *Biochim. Biophys. Acta* **599,** 552–568 (1980).
33. Zhang, M. *et al.* Calumin, a novel Ca^{2+}-binding transmembrane protein on the endoplasmic reticulum. *Cell Calcium* (in the press)..
34. Feramisco, J. D., Goldstein, J. L. & Brown, M. S. Membrane topology of human Insig-1, a protein regulator of lipid synthesis. *J. Biol. Chem.* **279,** 8487–8496 (2004).
35. Faulk, W. P. & Taylor, G. M. An immunocolloid method for the electron microscope. *Immunochemistry* **8,** 1081–1083 (1971).
36. Frank, J. *Three-dimensional Electron Microscopy of Macromolecular Assemblies* (Oxford Univ. Press, New York, 2006).
37. Harauz, G. & van Heel, M. Exact filters for general geometry three dimensional reconstruction. *Optik* **73,** 146–156 (1986).
38. Ma, J. Block by ruthenium red of the ryanodine-activated calcium release channel of skeletal muscle. *J. Gen. Physiol.* **102,** 1031–1056 (1993).
39. Takeshima, H. *et al.* Excitation-contraction uncoupling and muscular degeneration in mice lacking functional skeletal muscle ryanodine-receptor gene. *Nature* **369,** 556–559 (1994).
40. Li, E., Bestor, T. H. & Jaenish, R. Targeted mutation of the DNA methyltransferase gene results in embryonic lethality. *Cell* **69,** 915–926 (1992).